Carpathian Journal of Earth and Environmental Sciences, August 2020, Vol. 15, No. 2, p. 533 – 546; Doi:10.26471/cjees/2020/015/150

# MULTI-SCALE TEMPORAL PATTERNS IN SOIL RADON GAS DATA SERIES

**Gyozo JORDAN[1,2], & Silvana BELTRAN TORRES[1]**

[1] *Department of Applied Chemistry, Szent István University, Villányi út 35-43. 1118, Budapest, Hungary*
[2] Institute *for Geological and Geochemical Research, Hungarian Academy of Sciences, Budaörsi út 45, H-1112 Budapest, Hungary, corresponding author: gyozojordan@gmail.com, silvanybel@gmail.com*

**Abstract:** This paper reports on the applicability of wavelet analysis to the study of multi-scale temporal patterns in soil radon gas compared to the conventional time series analysis (TSA). Both methods delivered good modeling results for the studied 15 minutes sampled time series. The main achievement of the wavelet method is the identification and numerical characterization of the subtle semi-diurnal (12 h) periodicity. Unlike the other time series components (cycle, diurnal periodicity etc.), the semi-diurnal periodicity is the only temporal feature which is the same in the studied July (summer) and December (winter) time series.

**Keywords**: wavelet, time series analysis, modeling, monitoring, frequency

## 1. INTRODUCTION

The harmful health effect of radon is well-known (Nazaroff & Nero, 1988; WHO, 2009). Thus, its environmental occurrence and behavior has been intensively studied in the last decades. Radon in the soil is the major source of indoor radon and it is one of the bases of the geogenic radon potential calculation (Neznal et al., 2004). Geogenic radon potential (GRP) offers the possibility to identify radon-prone areas (Cinelli et al., 2019; De Cort 2010; Dubois et al., 2010; Gruber et al., 2013; Ielsch et al., 2010; Jónás et al., 2017; Jónás et al., 2018; Kemski et al., 2001). It is obvious that short-term and long-term variations of radon in the soil ($c_{soilRn}$) can affect the GRP determinations.

Many studies show clear temporal variation of $c_{soilRn}$ at depth of 0.8-1 m (Al-Shereideh et al., 2006; Richon et al., 2007; Sundal et al., 2008; Winkler et al., 2001; Szabó et al., 2013; Perrier et al., 2009; Baykut et al., 2010; Crockett et al., 2010). Investigators have used various methods to study temporal variations. For example, Al-Shereideh et al., (2006), Richon et al., (2007) and Sundal et al., (2008) characterized radon dynamics by visual interpretation of monitoring time series curves and they calculated the summer-winter ratio for seasonality, while Winkler et al., (2001) applied time series analysis techniques such as seasonal decomposition, auto-correlation and cross-correlation analyses. In our former study, we presented a detailed classical time series analysis (TSA) to describe the dynamics of $c_{soilRn}$ in terms of trend, cycle, periodicity, auto-correlation and random component in an additive mode (Szabó et al., 2013). Perrier et al., (2009) also calculated the ratio of summer and winter average and applied Fourier spectrum analysis to determine diurnal and tidal components. Baykut et al., (2010) and Crockett et al., (2010) used two spectral decomposition techniques, Empirical Mode Decomposition (EMD) and Singular Spectrum Analysis (SSA). However, wavelet analysis has been applied for the dynamics of radon in the soil only for seismological purposes (Nikolopoulos et al., 2012; Nikolopoulos et al., 2014).

In addition to radon analysis in soil, temporal variation of radon concentration has also been observed at different depth in boreholes, caves and underground laboratories (4, 10, 53 m and 1 km) (Steinitz & Piatibratova, 2010a,b; Barbosa et al., 2007; Mentes & Eper-Pápai, 2015; Steinitz et al., 2011; Steinitz et al., 2013). Moreover, Steinitz et al., (2013) used a closed canister experiment in a laboratory in a one-storied building to observe radon temporal patterns excluding meteorological effects. Nevinsky et al., (2018) among other methods used continuous wavelet spectrum analysis of radon in boreholes and springs. Yan et al., (2017) and Woith et al., (2011) applied discrete and continuous wavelet methods for radon and other parameters such as water temperature, spring discharge

rates and galactic cosmic rays in hot springs.

Wavelet analysis has been developed to tackle the shortcomings of other signal processing methods such as disability of treating non-linearity, non-stationarity (Daubechies, 1990) at various time scales, thus it offers a good method for analyzing complex multi-scale monitoring data. It is able to reveal characteristics of data that other techniques miss, such as breakdown points, discontinuities and self-similarity (Mallat, 1989; Lee & Yamamoto, 1994) due to its ability to perform local analysis. Wavelet analysis is a windowing technique with variable data length. It allows using long- and short-time intervals as well to obtain more precise low or high frequency information.

In a former study dynamics of soil gas radon ($c_{soilRn}$) at 0.8 m depth was studied by conventional time series analysis (TSA) (Szabó et al., 2013). The principal objective of this study is to characterize soil radon gas time series from the same location and to identify multi-scale temporal features and non-stationary localized features such as transient events benefitting from the flexible time series analysis capabilities of the wavelet analysis method. In this study, wavelet analysis results are compared to the conventional time series analysis results, while also evaluating its advantages and disadvantages.

## 2. MATERIALS AND METHODS

### 2.1. Soil radon time series data

The analyzed time series comes from the soil radon gas monitoring site in the Budapest urban area described in Szabó et al., (2013). The selected data corresponds to $c_{soilRn}$ measured at 0.8 m depth, every 15 min for 8 days (776 measurements) in July and 6 days (583 measurements) in December and the corresponding temperatures measured simultaneously in Centigrade degrees. The data selection criteria was based on the results found by Szabó et al., (2013) where the one-week measured signals were grouped in two seasonal clusters regarding their similarities in the amplitude and periodicity; winter from October to March (April was not measured) and summer from June to September (Szabó et al., 2013). In the present study, the signals from the July and December time series were chosen for wavelet analysis as representatives for the summer and winter seasons, respectively.

### 2.2. Wavelet analysis

Continuous wavelet transform (CWT) results in wavelet coefficients (C) calculated by summing the signal $f(t)$ multiplied by the scaled and shifted form of the wavelet function $\psi$ over time:

$$C(scale, position) = \int f(t)\psi(scale, position, t)dt \quad (1)$$

Scaling a wavelet means stretching it with a scale factor. The 'scale' is very similar to the wavelength (frequency) in the Fourier analysis and various 'scales' correspond to the wavelet stretched by different scale factors. Shifting the wavelet function $\Psi$ means moving it along the studied time series, in order to align $\Psi$ with the target feature of the time series, considering the delay or hastening (k) for the corresponding analysis which is expressed as f(t-k) (Misit et al., 2001). In the C coefficient plot, the x-axis represents time and the y-axis represents scale, while the color at each x–y point indicates the magnitude of C ('z axis') (see Figs 1 and 2).

The limitation of wavelet analysis is that the result can be dependent on the employed wavelet function. For example, an asymmetric signal type can be best analyzed with an asymmetric wavelet such as the Daubechies wavelet (db) or the nearly symmetric Symlet wavelet, while symmetric wavelets such as the Mexican Hat, the Gaussian Derivatives Family and the FIR Based Approximation of the Meyer Wavelet (dmey) are more suitable for symmetric signals such as a periodic sinusoidal wave. Also, some wavelets are very efficient in identifying sudden brakes in the signal such as the lower level Daubechies or the Haar (step function) wavelets, having short support (small moving window) (Misit et al., 2001). For the studied radon time series several wavelet functions were compared and the symmetric Meyer Wavelet (dmey) function was selected for the final analysis. The reasons that we chose dmey were:

1) it can perform both continuous and discrete analysis;

2) it is symmetric and thus it is similar to the radon time series curve around the local maxima and minima,

3) one of the objectives of the analysis was the identification and localization of the multi-scale regular periodicities where the dmey wavelet having long support performed the best,

4) the identification of sudden discontinuities in the high-frequency domain was not a target.

Compared to CWT, the discrete wavelet transforms (DWT) calculates C only for a subset of scales and positions without loss of information (Mallat, 1989). During the DWT the original signal (S) is passed through two complementary filters, resulting two signals: the approximations (A) are the high-scale (low-frequency) components of the signal, and the details (D) are the complementary low-scale (high-frequency) components (see Figures 3 and 4, for example). These filters are successively applied to the approximations emerging at increasing scales. The output of the DWT procedure is a series of approximations and

corresponding details at various scales.

In this study, both the continuous and discrete wavelet analyses use the dmey wavelet transform (Misit et al., 2001) implemented with the MATLAB® Wavelet Toolbox.

### 2.3. Conventional time series analysis (TSA)

Detailed description of the conventional time series analysis (TSA) on $c_{soilRn}$ time series can be find in Szabó et al., (2013). TSA defines pattern according to an additive decomposition of the radon measurement series into the following components: trend *T(t)*, cycle *C(t)*, periodicity *P(t)*, auto-correlation *A(t)*, white noise residuals *ε(t)* and the so called events *E(t)* which comprises outliers $E_O(t)$ and transient process $E_T(t)$ of the time series (Eq. (2)) (Tukey, 1977; Velleman & Hoaglin, 1981; Makridakis et al., 1998).

$$c(t) = T(t) + C(t) + P(t) + A(t) + E(t) + \varepsilon(t) \quad (2)$$

In this investigation, TSA results are compared to wavelet analysis in terms of trend, cycle, periodicity and the random noise in order to evaluate advantages and disadvantages of the wavelet method.

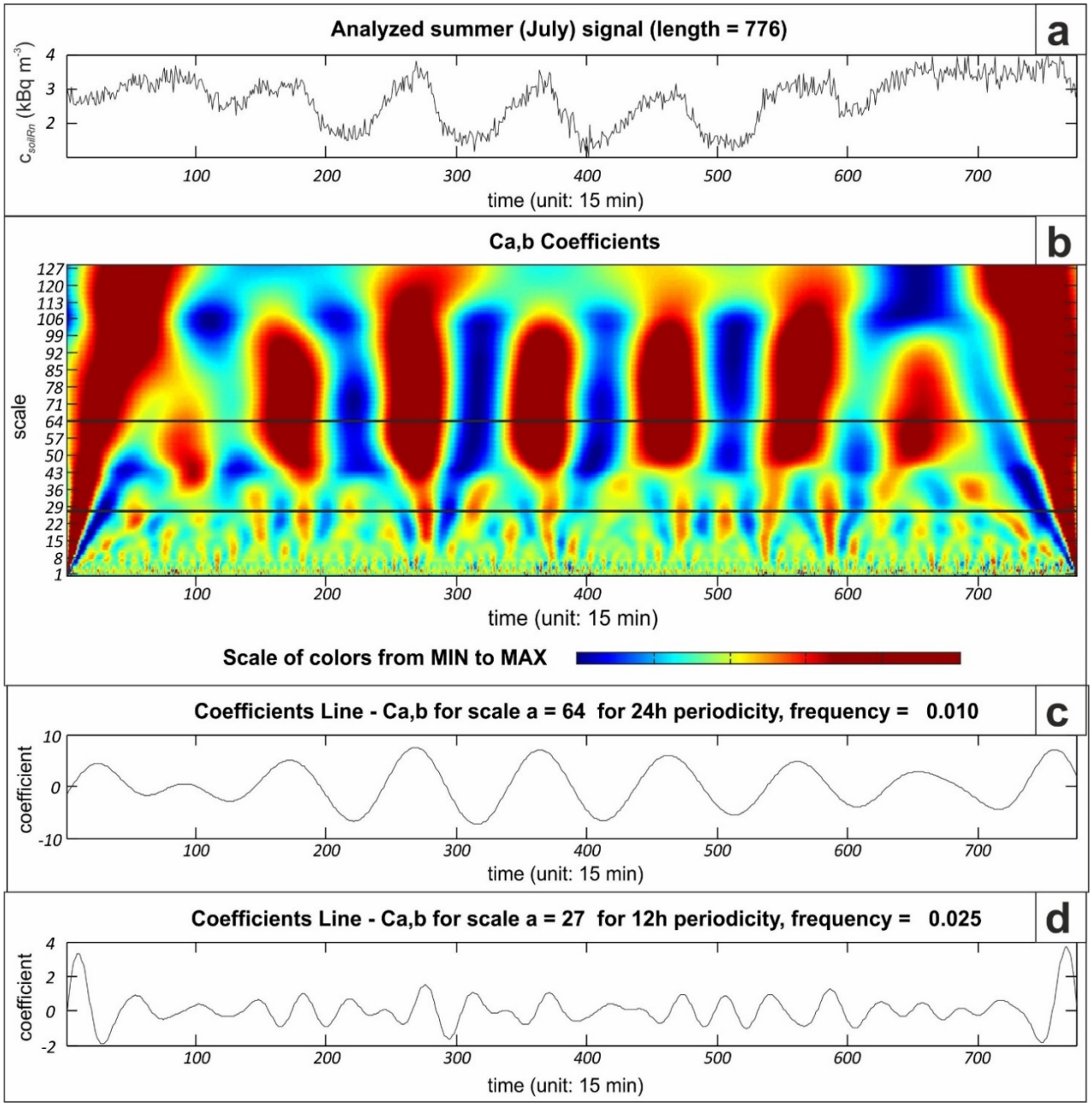


Figure 1. Result of the continuous wavelet transform using the Meyer 'dmey' wavelet, for summer (July) soil radon gas activity concentration time series. a. Analyzed signal. b. Coefficients plot. c. Coefficients line at scale 64 corresponding to the 24 h periodicity. d. Coefficients line at scale 27 corresponding to the12 h periodicity.

## 3. RESULTS

### 3.1. Continuous wavelet analysis

The plot of the continuous wavelet transform coefficients for summer (July) $c_{soilRn}$ (Fig. 1b) clearly display the horizontal series of vertically elongated zones of local maxima in red and minima in blue, showing periodicity about every 100 measurements in X axis (Fig. 1a, 1b), that is approximately 96, which is the exact number of measurements taken every 15 min in 24-hour long diurnal period and its frequency is 0.01. To connect all maxima and minima zones corresponding to the 24 h periodicity, a horizontal line was traced in the CWT diagram based on visual inspection, which corresponds to scale 64 in the Y axis (Fig. 1b). The coefficient line constructed across the 24 h local minima and maxima shows the highly regular diurnal periodic feature in the summer season (Fig. 1c). A similar regular periodic pattern emerges in the coefficients constructed across the 12 hour local minima and maxima that corresponds to scale 27 in Y axis (Fig. 1d) and 0.025 frequency.

The CWT plot of the coefficients for the winter (December) $c_{soilRn}$ displays a picture very different from the one observed for summer (July) (Fig. 2a). The 24 hours periodicity is poorly localized in the

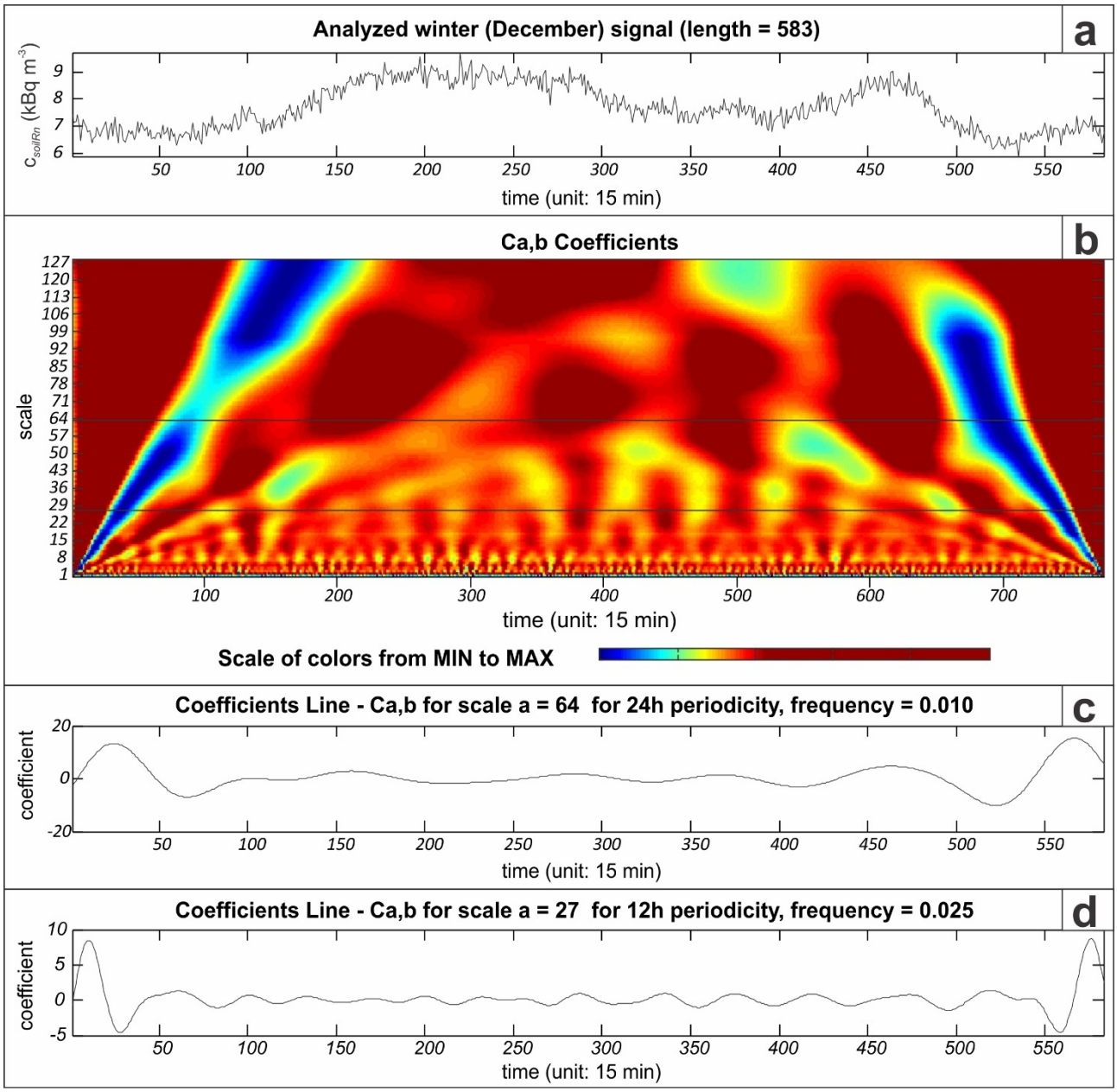


Figure 2. Result of the continuous wavelet transform (CWT; using the Meyer 'dmey' wavelet) for winter (December) soil radon gas activity concentration time series. a. Analyzed signal. b. Coefficients plot.. c. Coefficients line at scale 64 corresponding to the 24 h periodicity. d. Coefficients line at scale 27 corresponding to the 12 h periodicity.

temporal and frequency domains and it appears rather irregular and blurred (Fig. 2b). The corresponding coefficient line is also irregular both in periodicity and in amplitude (Fig. 2c). However, the 12-hour period remains well defined both in time and scale similar to the summer (July) radon time series (Fig. 2d)

### 3.2. Discrete wavelet analysis

#### 3.2.1. High-frequency component ('residuals')

No interpretable auto-correlation was found in the outlier free first detail (D1, Fig. 3) of the discrete wavelet transform (DWT) of the studied summer (July) $c_{soilRn}$ time series. Although auto-correlation was found in the D1 series at the first three time lags significant at the 95% confidence level, all were small between r =-0.5 and r =0.2. This indicates the high variability of $c_{soilRn}$ and the lack of a relationship between measurements taken at successive 15 min intervals. Also, no significant trend was detected in this detail. The D1 time series (Fig. 3) had a zero average and median (at the 95% confidence level) with homogeneous and symmetric distribution. Thus, the finest detail D1 represents the high frequency random component of the studied $c_{soilRn}$ series. When the outlier free D1 series is compared to the outlier free random residuals of the conventional TSA (Szabó et al., 2013) no statistically significant difference is found between the median, average, and the distributions according to the Mann-Whitney Test, T-test and the Kolmogorov-Smirnov Test, respectively. The median of the differences between the two time series is negligible (0.06 kBq $m^{-3}$). The similarity of the two random series is confirmed by their moderately strong correlation (r=0.76). The lack of cross-correlation also supports the similar random nature of the two high-frequency series. Thus, there is no statistically significant difference between the wavelet analysis and the conventional TSA residuals and both methods provide good models of the studied soil radon gas activity concentrations.

The winter (December) first detail D1 series has the same characteristics as the summer (July) D1 series (Fig. 4). The only difference between the summer and winter high frequency D1 outlier free random components is in their variability: the summer values range between -0.32 and 0.32 kBq $m^{-3}$ (range = 0.64

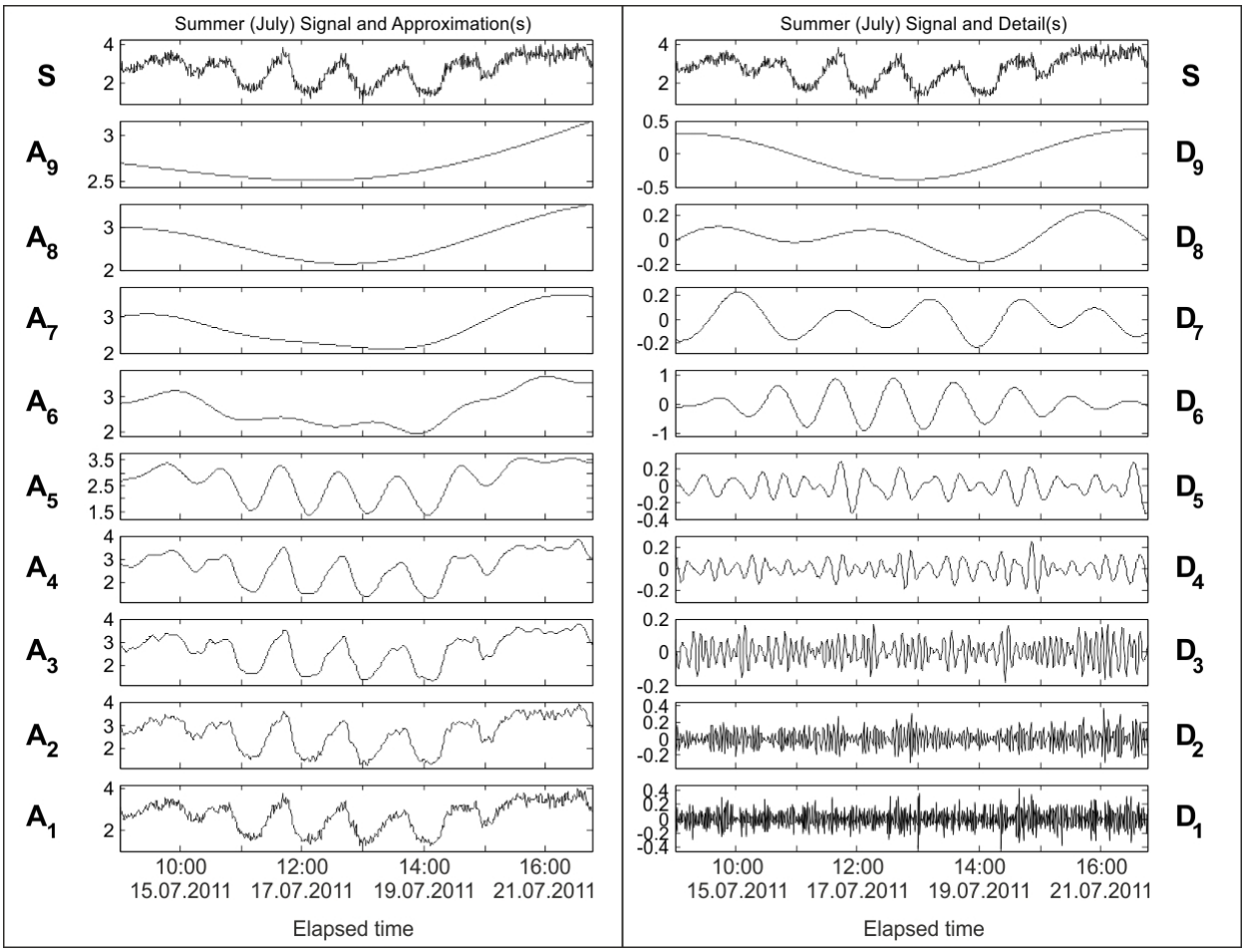


Figure 3. Result of the DWT uding Meyer 'dmey' wavelet, for summer (July) soil radon gas activity concentration (kBq $m^{-3}$) time series. S is the studied signal. A1-A9: approximations, D1-D9: details. D6 is the 24 h periodicity, D5 is the 12 h periodicity.

kBq $m^{-3}$) and the winter values range between -0.45 and 0.47 kBq $m^{-3}$ (range =0.92 kBq $m^{-3}$) (Figs 3 and 4). This shows that winter extreme variability is higher than in summer by 36%, thus, winter radon activity concentration dynamics seems to be more variable and hence less predictable. The overall stochastic variability of soil radon activity concentration is significantly higher in winter than in summer as confirmed by the F Test at the 95% confidence level.

### 3.2.2. Periodicity

The diurnal (24 h) periodicity is revealed by the D6 detail both in summer and winter seasons (Figs 3 and 4). The 24 h periodicity is quantified in the frequency domain both by the single peak periodogram and by the regular auto-correlogram for D6 (summer: Figs 5e and 5g and winter: 5f and 5h).

The summer (July) D6 detail is highly regular in the frequency domain (i.e. the curve has constant stationary wavelength) as the time period between successive local extremes range between 94-100 measurements with an average of 97 measurements taken every 15 minutes (97 x 15 minutes = 1425 minutes = 23.75 hours) (Fig. 5a). The sine wave fitted by the least-squares method models well the average behavior of the D6 details. The coincidence of the original D6 details and the fitted sine curve also shows a marked periodicity of the radon time series in summer (Fig. 5c). However, the D6 periodic curve is strongly varying in amplitude as the minimum and maximum amplitudes differ by 0.8 kBq $m^{-3}$, which is 150% of the average absolute amplitude magnitude (0.55 kBq $m^{-3}$) (Fig. 5a).

When the D6 detail is compared to the conventional TSA diurnal periodic component, very little difference is found for the summer season (July) (Fig. 5a). For example, the largest discrepancies occur at the local maxima and minima but the difference between the two curves, even at these locations, remain small (0-0.46 kBq $m^{-3}$). There is a high similarity between the two models (D6 detail and TSA diurnal curve) in the frequency domain (wavelength): the location of the local extremes differs only by 0.5-2.75 hours (Fig. 5a). Also, there is essentially no difference between the two sine curves fitted to the wavelet D6 detail and the diurnal TSA curve: they are in perfect phase, they have the same periodicity (24 h = 96 measurements) and the difference between the two sine curve amplitudes is a

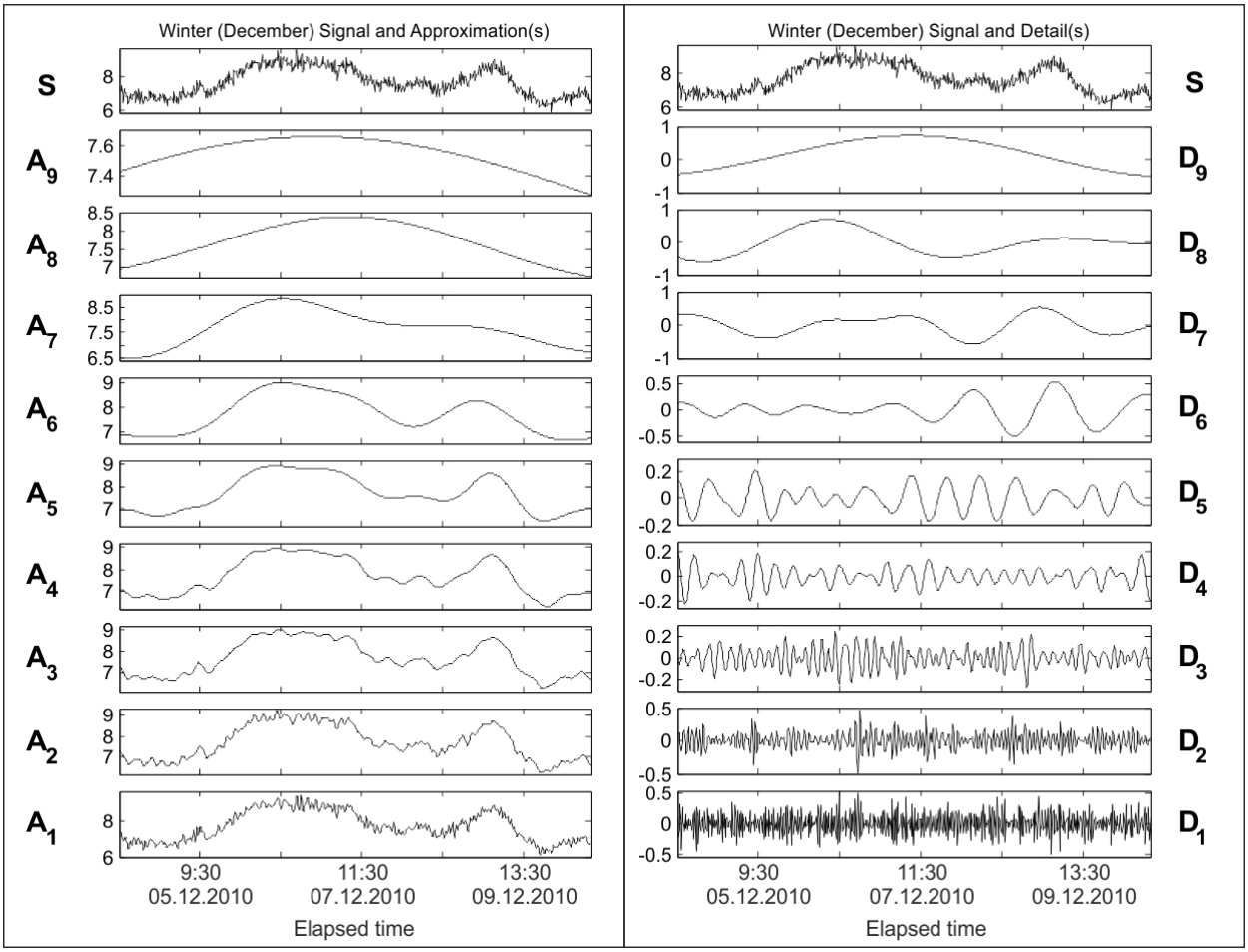


Figure 4. Result of the DWT using Meyer 'dmey' wavelet for winter (December) soil gas radon activity concentration time series. S is the studied signal. A1-A9: approximations, D1-D9: details. D6 is the 24 h periodicity, D5 is the 12 h periodicity.

small value of 0.08 kBq m$^{-3}$ (13% difference only) (Fig. 5). A closer look at the periodic curves of the two methods shows that while the wavelet curve (D6) is highly regular and smooth, the conventional TSA curve reveals the subtle asymmetry of the diurnal radon activity concentration time series (Fig. 5a). Asymmetry is measured by the average difference of the length of the rising and falling limbs in the evaluated periods. Unlike in the near symmetric D6 series, which have a 11.75 h long daily increase and a 12.25 h long daily decrease, the daily increase of the radon activity concentration is slower (14.25 h) than the subsequent decrease (8.75 h) during the daytime according to the conventional TSA asymmetric series. The comparison of these two time spans shows a 9% larger asymmetry of the TSA compared to the D6 series (Fig. 5a). This phenomenon of asymmetric rising and falling limbs in the diurnal period was also demonstrated by Barbosa et al., (2015) for radon activity concentration in a remediated tailings of

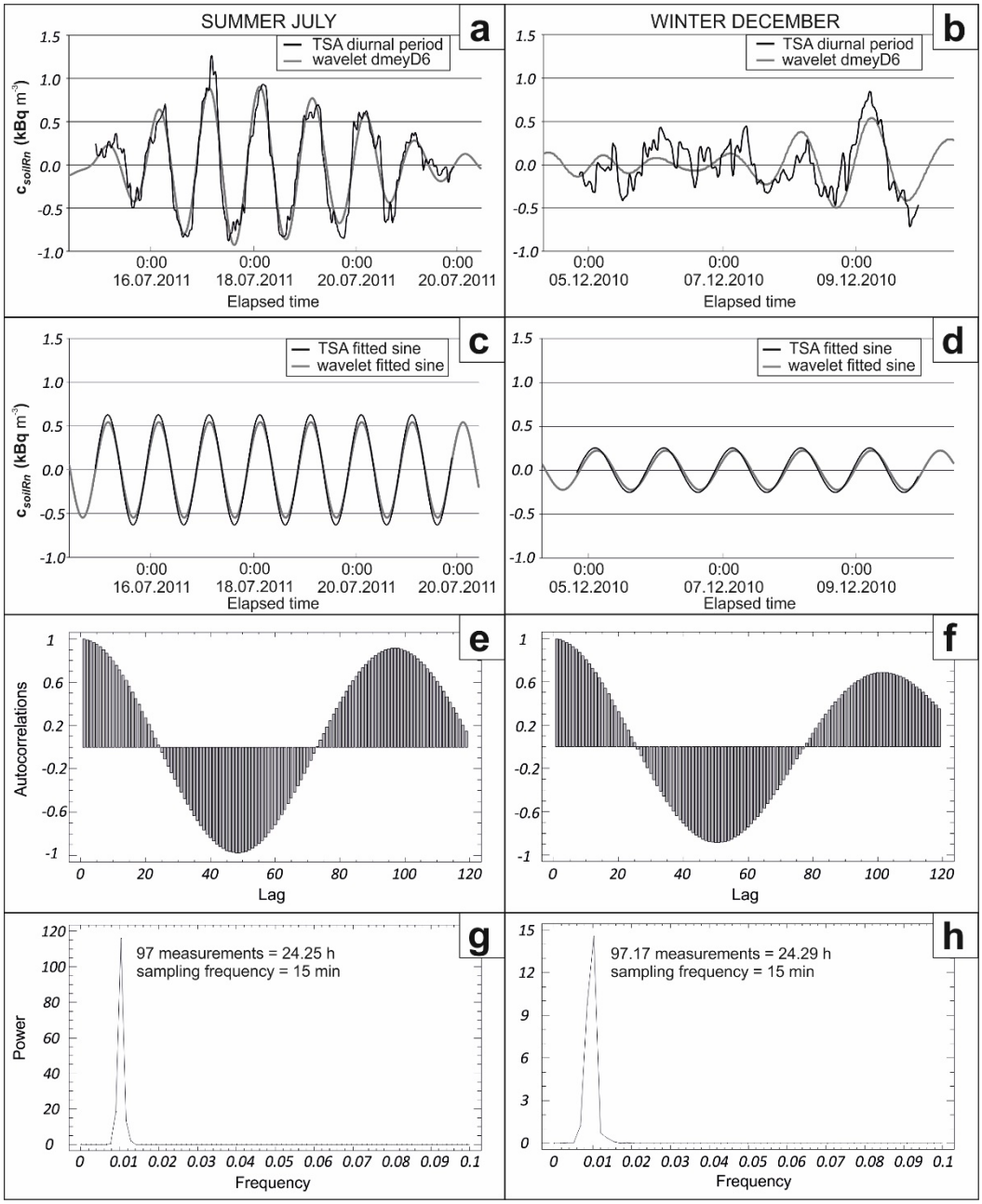


Figure 5. Comparison of conventional TSA analysis and wavelet analysis of the diurnal periodicity of soil gas radon activity concentration (kBq m$^{-3}$). a, b. Diurnal periodicities from the two analyses for the summer (July) and winter (December) time series. c, d. The least-squares fitted sine waves to the diurnal periodicities of the two analyses for the summer (July) and winter (December) time series. e, f. Auto-correlograms of the diurnal periodicity for the summer (July) and winter (December) for the two analyses. g, h. Periodograms of the diurnal periodicity for the summer (July) and winter (December) for the two analyses.

uranium mine. They found that the diurnal variability is strongly asymmetric, increasing slowly and decreasing faster.

The winter (December) curve, unlike the summer curve, is irregular in the frequency domain (wavelength) and the local extremes fluctuate in the wide range of periods 75-112 measurements with an average of 95 measurements (23.75 hours), which is 6.5 time larger than in summer (Fig. 5b). The non-stationary periodicity (wavelength) of the winter soil radon activity concentration (Fig. 5b) is obvious when compared to the sine wave fitted by the least-squares method (Fig. 5d). Typically, while the average period is exactly one day (96 measurements), the maximum difference between the local extremes of the two curves (D6 and fitted sine wave) is as large as 4.5 hours (18 measurements). The periodic curve is also strongly non-stationary in the amplitudes as the minimum and maximum amplitudes of the wavelet D6 have a difference of 1.04 kBq $m^{-3}$ corresponding to 473% of the average amplitude of 0.22 kBq $m^{-3}$, which is 3 times larger than in summer (Fig. 5b).

When the winter D6 is compared to the conventional TSA diurnal component a large difference is found both in the frequency and amplitude (Fig. 5b). For example, the largest discrepancies in the amplitude occur at the local maxima and minima ranging between (0-0.55 kBq $m^{-3}$). The difference in the frequencies (wavelenths) as measured by the difference between the corresponding extreme locations is as large as 0.25-5.5 hours in winter, which is 2.3 times higher than in summer. However, there is essentially no difference between the two sine curves fitted to D6 and TSA diurnal component: they are in perfect phase having regular and uniform frequency (96 measurements) and the difference between the two amplitudes is 0.03 kBq $m^{-3}$. This difference is only 13% of the sine wave amplitude exactly like the summer period. A closer look at the periodic curves of the two methods shows that while the wavelet curve (D6) is highly regular and smooth the conventional TSA curve reveals the subtle asymmetry of the diurnal radon activity concentration change (Fig. 5b). Unlike in the essentially symmetric D6 series with a 12.38 h long daily increase and a 12.75 h long daily decrease, the daily increase of the radon activity concentration is slower (13.25 h) than the subsequent decrease (10 h) during the daytime according to the conventional TSA asymmetric series. The comparison of these two time spans shows a 17% larger asymmetry of the TSA compared to the D6 series which is almost a double of the summer period asymmetry (9%).

If we compare the diurnal DWT curves (D6) for the summer (July) and the winter (December) periods interesting features emerge with respect to soil radon gas activity concentration dynamics (Fig. 5). The overall periodic features are modeled by the fitted sine waves (Figs 5c and 5d). In Figs 5c and 5d it can be seen that the overall amplitude of the atmospheric conditions-driven diurnal periods is 2.5 times higher in July (amplitude=0.55 kBq $m^{-3}$; Fig. 5c) than in December (0.22 Bq $m^{-3}$; Fig. 5d). The wavelength of the fitted sine waves modeling the diurnal periodicity for summer and winter are very similar, 24 h (96 measurements) and 24.25h (97 measurements) respectively. However, a closer look at the original diurnal D6 DWT curves reveal localized non-stationary features (Figs 5a and 5b). The periodicity in summer is regular, however, the amplitude changes 150% in the short studied one-week time span. The winter periodic model is much more non-stationary than the summer one having 473% change in the amplitude and 39% change in the wavelength studied for one week. The higher irregularity in the frequency and amplitude of the winter period results in that this component is less predictable in winter: there is a much larger difference between the conventional TSA and wavelet models in winter than in summer (Figs 5a and 5b).

In addition to the diurnal (24 h) periodicity, the applied wavelet analysis revealed a 12 h semi-diurnal periodicity in the DWT D5 detail both in the summer and winter soil radon gas activity concentrations (Figs 6a and 6b). This shows that the signal processing capabilities of the wavelet analysis are superior to the conventional TSA which failed to identify this short term periodic component (Szabó et al., 2013). Beyond the visual recognition, the periodograms and auto-correlograms unambiguously quantify the half-day periodicity in the studied summer (periodogram peak at 13.86 h wavelength; Figs 6e and 6g) and winter (periodogram peak at 11.21 h wavelength; Figs 6f and 6h) DWT D5 time series. More interesting is the high similarity of the 12 h semi-diurnal periodic curves in the two seasons (Figs 6a and 6b). The median absolute amplitudes are very similar (0.14 for summer and 0.12 for winter), and for the fitted overall sine wave amplitudes are essentially identical (0.098 for summer and 0.091 for winter; Fig. 6d). The calculated wavelengths of the sine waves are 14.34 and 12.56 for summer and winter, respectively. In summary it can be stated that at the half-day (12 h) periodic scale there is no difference between the two seasons, although the summer radon activity concentration change seems a bit more irregularly shaped than that for winter (Fig. 6c). This temporal feature is the only one exhibiting no difference between the two seasons.

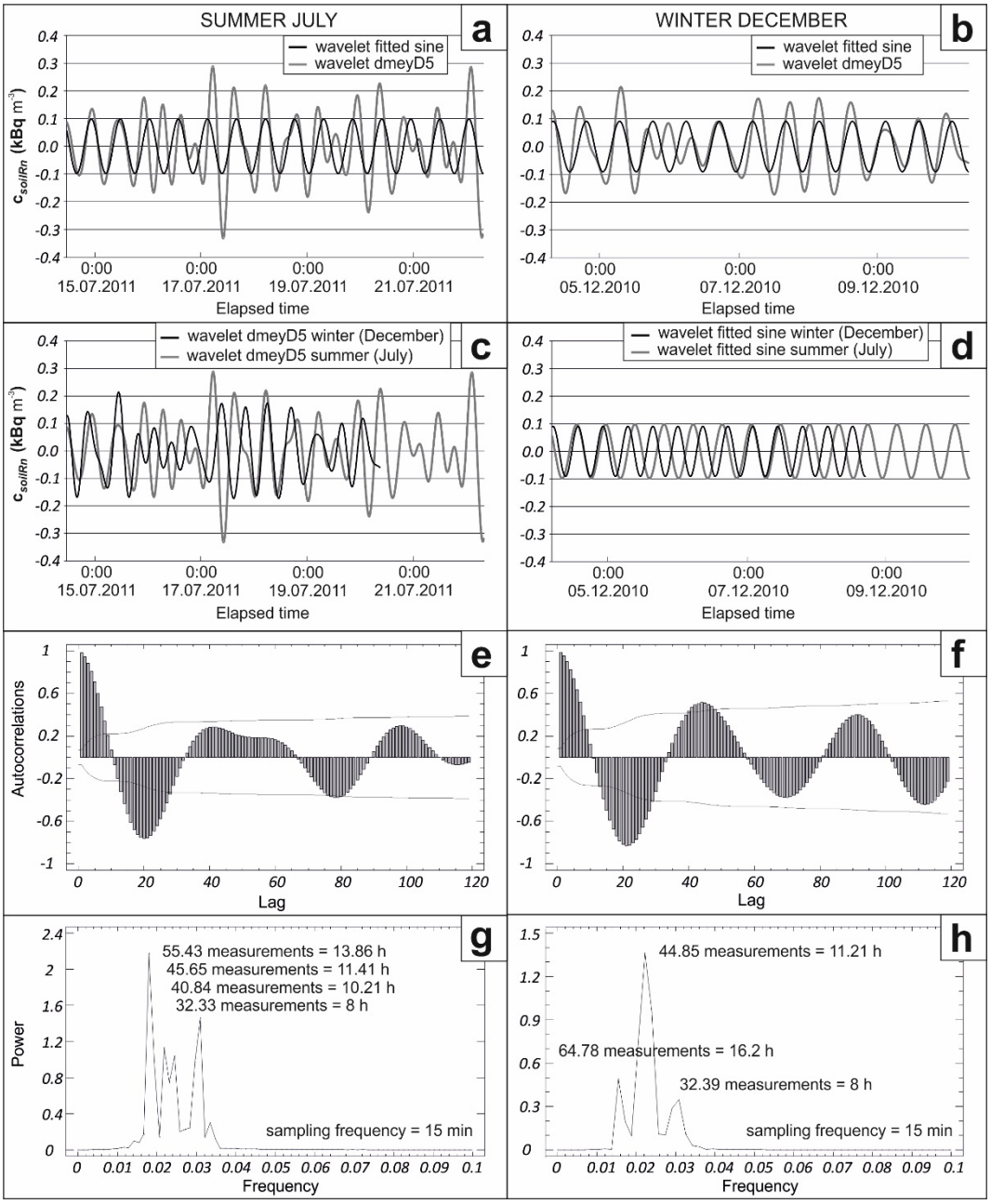


Figure 6. The 12 h semi-diurnal periodicity in the DWT D5 detail in the summer (July) (a) and winter (December) (b) soil radon gas activity concentration time series with the fitted sine waves. c. Comparison of the 12 h semi-diurnal periodicity in the summer (July) and winter (December) seasons. d. Comparison of the least-squares fitted sine waves for the 12 h semi-diurnal periodicity in the summer (July) and winter (December) seasons. e, f. Auto-correlograms of the 12h periodicity for the summer (July) and winter (December) for the two analyses. g, h. Periodograms of the 12h periodicity for the summer (July) and winter (December) for the two analyses.

Additionally, other less significant periods are visible at the 11.41 h, 10.21 h and 8 h and at the 16.2 h and 8 h periods in summer and winter, respectively. The 8 h period was identified with the known compartment of the solar tide by other studies (Mentes G & Eper-Pápai, 2015; Steinitz et al., 2011).

### 3.2.3. Cycle

Cycle, unlike period, is a recurrent phenomenon without fixed period (wavelength). The two studied seasonal radon activity concentration time series reveal a cycle component in the higher details (D9 in summer and D8 in winter) with two local minima or maxima indicating a half-week (ca. 84 hours) 'periodicity' (Figs 7a and 7b). When the cycles modeled by the wavelet analysis and by the conventional TSA are compared the median difference in summer is 80%, while it is as high as 200% in winter. This shows that the cycle component in the radon activity concentration, too, is less predictable in the winter

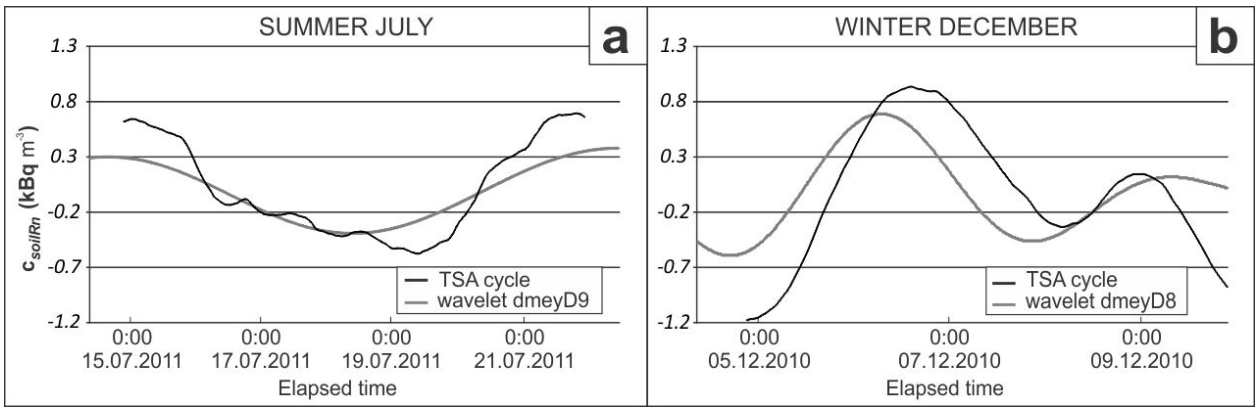


Figure 7. Comparison of conventional TSA analysis and wavelet analysis of the cycle of soil gas radon activity concentration in the summer (July) (a) and winter (December) (b).

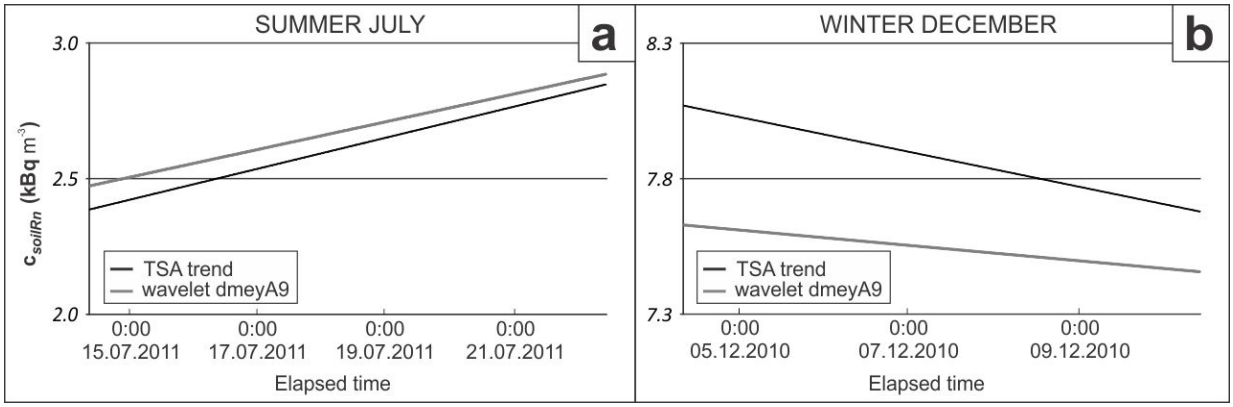


Figure 8. Result of the comparison of conventional TSA analysis and wavelet analysis of the trend of soil gas radon activity concentration in the summer (July) (a) and winter (December) (b).

season, similar to the diurnal period. It is interesting that the maximum amplitude of the winter cycle (0.93 Bq m$^{-3}$) is higher than in summer (0.39 Bq m$^{-3}$).

### 3.2.4. Trend

Finally, the trend analysis shows significant linear trend in the wavelet highest scale approximations (A9) both in winter and summer (Figs 8a and 8b). The linear trends obtained from the conventional TSA show no statistically significant difference from the wavelet-based trend analysis at the 95% confidence level. However, the two trend models in winter have a higher discrepancy than those fitted to the summer radon activity concentration time series, suggesting less predictability and hence higher uncertainty in the trend component as well in the winter soil gas radon activity concentration.

## 4. DISCUSSION

Evaluating the performance of the wavelet analysis in comparison to the conventional TSA, it can be stated that both methods deliver good modeling results as measured by the model random residuals (the highest frequency components). The residuals of both methods are random time series with no statistically significant difference between their distributions, both in summer and winter.

Both continuous and discrete wavelet analysis and also the conventional TSA readily identified the dominant 24 h diurnal period, although, the discrete wavelet D6 curve is smoother and more regular than the conventional TSA curve. But, this curve, computed using the dmey wavelet transform did not capture the asymmetry in the daily fluctuations, unlike the conventional TSA method. Both methods could identify the non-stationary features of the studied soil radon gas time series.

The discrepancy between the two modeling methods is larger in the winter season both in the amplitude and frequency of the diurnal periodicity than in the summer season. The higher regularity and predictability of the observed soil gas radon activity concentration dynamics in summer is caused by the single dominating effect of the atmospheric processes such as the strong diurnal surface temperature alterations (Szabó et al., 2013). In the absence of the overwhelming atmospheric processes in winter, the very complex soil pore conditions result in a much more hectic behavior of soil radon gas.

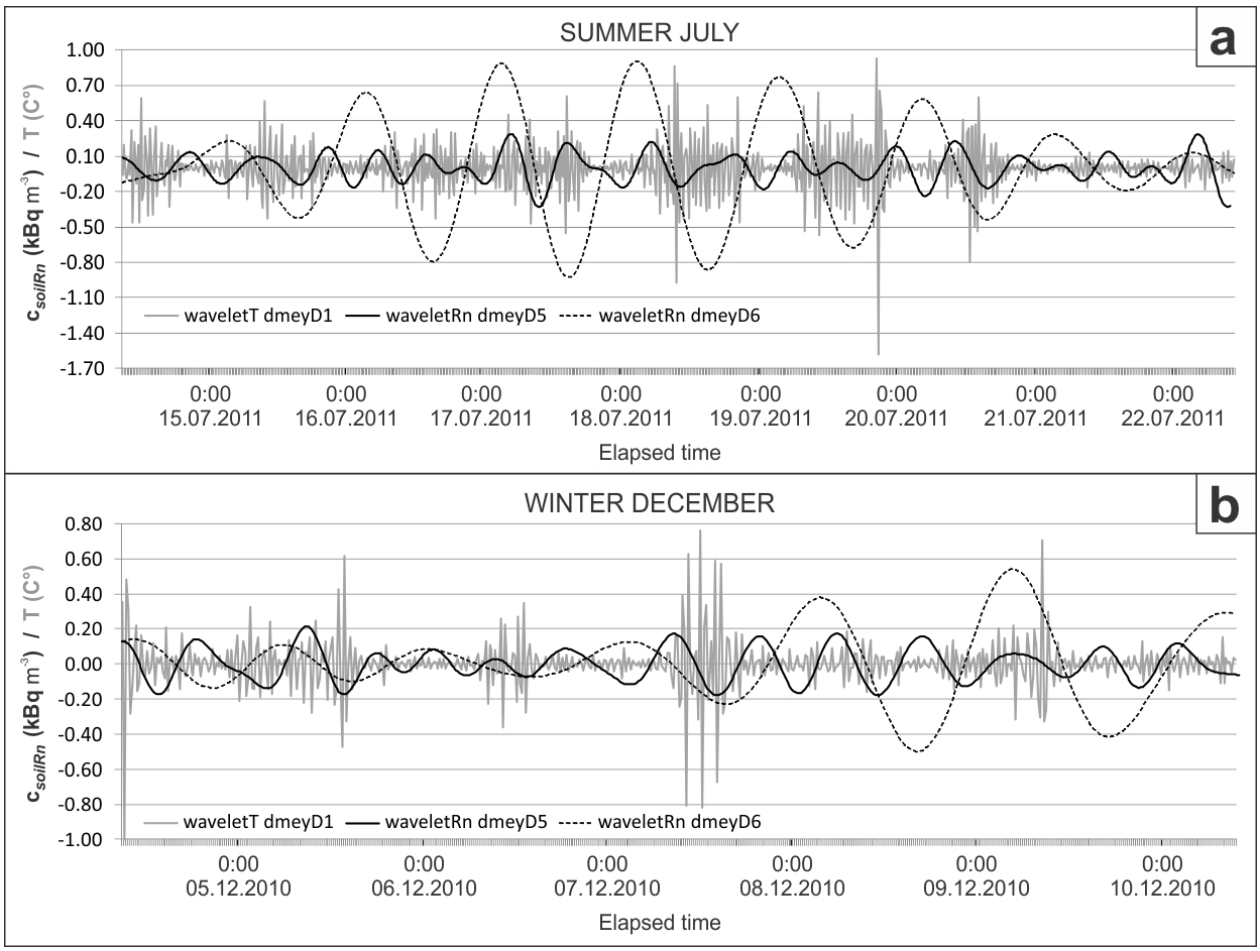


Figure 9. The diurnal (waveletRn dmeyD6) and semi-diurnal (waveletRn dmeyD5) periodicity of soil gas radon activity concentration (kBq m$^{-3}$) and the local variability in the high frequency random component of the simultaneously measured atmospheric temperature (waveletT dmeyD1) for summer (July) (a) and winter (December) (b) seasons.

The comparison of the seasonal DWT diurnal curves also shows the higher magnitude and regularity of the atmospheric conditions-driven diurnal periodicity in the summer season.

The main achievement of the soil radon gas time series analysis by the wavelet method is the identification and numerical characterization of the subtle semi-diurnal (12 h) periodicity. Unlike the other time series components such as trend, cycle, diurnal periodicity and high-frequency 'residuals', the semi-diurnal 12 h periodicity is the only temporal feature which is the same in both the summer and winter seasons. This shows that this periodic process is independent from atmospheric conditions. This can be explained by the gravitational force of the Moon and the Sun exerted on Earth's porous rock and soil media, resulting in periodic contraction of the pore space, affecting the soil radon gas partial pressure. Another explanation could be given by resorting to solar irradiation changes, which directly affect this behavior, as it was shown by many other studies (Perrier et al., 2009; Mentes G & Eper-Pápai, 2015; Steinitz et al., 2011). The simultaneously measured atmospheric temperature data also confirms this finding. Figs 9a and 9b show the diurnal (wavelet transform of radon gas time series at 24 h periodicity - waveletRn dmeyD6) and semi-diurnal (wavelet transform of radon gas at 12 h periodicity waveletRn dmeyD5) periodicity of $c_{soilRn}$ and the local variability in the high frequency random component of the atmospheric temperature (waveletT dmeyD1) for summer (July) and winter (December) seasons, respectively. It can be seen that the 12 h periodicity is independent from the diurnal or seasonal atmospheric temperature changes.

Soil radon gas is a highly sensitive tracer of secondary geodynamic processes according to Steinitz et al., (2011). Several studies suggest that gravitational tides have an influence on soil radon gas variability, since both earth tides and ocean tidal loading may cause periodic radon exhalation via crustal expansion and compression and via geophysically-driven groundwater level variations (Crockett et al., 2010; Aumento, 2002; Groves-Kirby et al., 2006; Weinlich et al., 2006). Steinitz et al., (2013) measured tidal and diurnal periodicity in radon time series in a 1 km deep

underground laboratory, indicating an extra-terrestrial gravitational driving mechanism (Steinitz et al., 2013). This result was also confirmed by Steinitz et al., (2011) who stated that the periodic phenomena of the rotation of earth around its axis and around the sun causes only the compound association among the amplitudes and phases of the diurnal and seasonal periodicities of the daily $c_{soilRn}$ signal. Radon variation patterns in the frequency domain cannot be driven by the atmospheric variation patterns, according to these investigators. They also stated that this extra-terrestrial influence, which drives the daily signals of radon inside a closed canister, is non-atmospheric and seemed to be from a remote source (Steinitz et al., 2011).

Both the wavelet analysis of this study and conventional TSA (Szabó et al., 2013) identified similar half-week cycles in the same soil gas radon activity concentration time series. Steinitz et al., (2011; 2013) also found non-periodic multi-day (2-10 days) cycles. In the present study, the difference between the two modeling results is larger for the half-week cycle in winter than in summer, again, due to the higher variability of soil gas radon at the multi-day time scale in winter. Szabó et al., (2013) studied weekly time series and found the half-week period throughout the year.

Regarding the longest term change, both methods identified the same trends, although the higher difference occurred in the winter season supporting that the winter soil gas radon activity concentration dynamics is less predictable.

## 5. CONCLUSIONS

This study shows that all the time series features such as trend, cycle, diurnal periodicity and high-frequency random noise are consistently different in the studied July and December time series representing summer and winter seasons. The most interesting finding is that the semi-diurnal 12 h feature is independent from seasonal atmospheric variations. In term of the wavelet analysis efficiency, this technique was successful in capturing the non-stationary features of the soil gas radon monitoring time series. According to this study, the signal processing capability of wavelet analysis seems to be superior to the conventional TSA which failed to identify this short term (semi-diurnal) periodic component.

**Acknowledgements**

This research has been supported by the National Research, Development and Innovation Fund – NKFIA, TÉT_16-1-2016-0087. The National Research, Development and Innovation Office – NKFI (OTKA) Fund No. SNN118101 and the EU INTERREG Danube Transnational Programme (DTP2-093-2.1) SIMONA funds are also acknowledged. Katalin Szabo's important contribution is gratefully acknowledged. This paper reports on the research at the GEM-RG Geochemistry, Modelling and Decisions Research Group. This study was greatly inspired by motivating discussions with Susana Barbosa and Gideon Steinitz.

## REFERENCES

**Al-Shereideh, S.A., Bataina, B.A. & Ershaidat, N.M.,** 2006. *Seasonal variations and depth dependence of soil radon concentration levels in different geological formations in Deir Abu-Said district, Irbid - Jordan.* Radiat Meas. 41:703-707

**Aumento, F.,** 2002. *Radon tides on an active volcanic island: Terceira, Azore*. Geofís Int. 41:499-505

**Barbosa, S.M., Lopes, F., Correia, A.D., Barbosa, S., Pereira, A.C. & Neves, L.F.,** 2015. *Temporal variability of radon in a remediated tailing of uranium ore processing - the case of Urgeiriça (central Portugal).* J Environ Radioactiv. 142:14-23

**Barbosa, S.M., Steinitz, G., Piatibratova, O., Silva, M.E. & Lago P.,** 2007. *Radon variability at the Elat granite, Israel: Heteroscedasticity and nonlinearity.* Geophys Res Letters. 34, L15309, doi:10.1029/2007GL030065

**Baykut, S., Akgül, T., Inan, S. & Seyis, C.,** 2010. *Observation and removal of daily quasi-periodic components in soil radon data.* Radiat Meas. 45:872-879

**Cinelli, G., Tollefsen, T., Bossew, P., Gruber V., Bogucarskis, K., De Felice L. & De Cort M.,** 2019. *Digital version of the European Atlas of natural radiation.* J Environ Radioactiv. 196:240-252

**Crockett, R.G.M., Perrier, F. & Richon, P.,** 2010. *Spectral-decomposition techniques for the identification of periodic and anomalous phenomena in radon time-series.* Nat Hazard Earth Sys. 10:559-564

**Daubechies, I.,** 1990. *The wavelet transform, time-frequency localization and signal analysis.* IEEE Transactions on Information Theory, 36:961-1005

**De Cort, M. (Ed.),** 2010. *Advances in Radon Mapping.* J Environ Radioactiv. 101:785-894

**Dubois, G., Bossew, P., Tollefsen, T. & De Cort, M.,** 2010. *First steps towards a European atlas of natural radiation: status of the European indoor radon map.* J Environ Radioactiv. 101:786-798

**Durridge Company Inc. RAD7 Electronic Radon Detector**, 2000. User Manual

**Groves-Kirby, C.J., Denman, A.R., Crockett, R.G., Phillips, P.S. & Gillmore, G.K.,** 2006. *Identification of tidal and climatic influences within domestic radon time series from Northamptonshire, UK.* Sci Total Environ. 367:191-202

**Gruber, V., Bossew, P., De Cort, M. & Tollefsen T.**,

2013. *The European map of the geogenic radon potential*. J Radiol Prot. 33:51-60

**Ielsch, G., Cushing, M.E., Combes, Ph. & Cuney, M.,** 2010. *Mapping of the geogenic radon potential in France to improve radon risk management: methodology and first application to region Bourgogne*. J Environ Radioactiv. 101:813-820

**Jónás, J., Somlai, J., Csordás, A., Tóth-Bodrogi, E. & Kovács, T.,** 2018. *Radiological survey of the covered and uncovered drilling mud depository.* J Environ Radioactiv. 188:30-37

**Jónás, J., Somlai, J., Tóth-Bodrogi, E., Hegedűs, M. & Kovács, T.,** 2017. *Study of a remediated coal ash depository from a radiological perspective.* J Environ Radioactiv. 173:75-84

**Kemski, J., Siehl A., Stegemann, R. & Valdivia-Manchego, M.,** 2001. *Mapping the geogenic radon potential in Germany.* Sci Total Environ. 272:217-230

**Lee, D.T.L. & Yamamoto, A.,** 1994. *Wavelet analysis: Theory and applications.* Hewlett-Packard Journal. 45:44-54

**Makridakis, S.G., Wheelwright, S.C. & Hyndman, R.J.,** 1998. *Forecasting: Methods and Applications*, third ed. Whiley Publisher, New York

**Mallat, S.,** 1989. *A theory for multiresolution signal decomposition: The wavelet representation: IEEE Trans.* Pattern Analyse Mache Intelligent, 31:674-693

**Mentes, G. & Eper-Pápai, I.,** 2015. *Investigation of temperature and barometric pressure variation effects on radon concentration in the Sopronbánfalva Geodynamic Observatory, Hungary*. J Environ Radioactiv. 149:64-72

**Misit, M., Misit, Y., Oppenheim, G. & Poggi, J.M.,** 2001. *Wavelet Toolbox for use with MATLAB*. http://www.mathworks.com

**Nazaroff, W.W. & Nero, Jr. A.V.,** 1988. *Radon and its decay products in indoor air, United States of America*: John Wiley & Sons

**Nevinsky, I., Tsvetkova, T., Dogru, M., Aksoy, E., Inceoz, M., Baykara, O., Kulahci, F., Melikadze, G., Akkurt, I., Kulali, F., Vogiannis, E., Pitikakis, E., Katsanou, K. & Lambrakis, N.,** 2018. *Results of the simultaneous measurements of radon around the Black Sea for seismological applications.* J Environ Radioactiv. 192:48-66

**Neznal, M., Neznal, M., Matolin, M., Barnet, I. & Miksova, J.,** 2004. *The New Method for Assessing the Radon Risk of Building Sites.* In: Czech Geol. Survey Special Papers, vol. 16. Czech Geol. Survey, Prague. http://www.radon-vos.cz/pdf/metodika.pdf

**Nikolopoulos, D., Petraki, E., Marousaki, A., Potirakis, S.M., Koulouras, G., Nomicos, C., Panagiotaras, D., Stonhamb, J. & Louizif, A.,** 2012. *Environmental monitoring of radon in soil during a very seismically active period occurred in South West Greece*. J Environ Monit. 14:564

**Nikolopoulos, D., Petraki, E., Vogiannis, E., Chaldeos, Y., Yannakopoulos, P., Kottou, S., Nomicos, C. & Stonham, J.,** 2014. *Traces of self-organisation and long-range memory in variations of environmental radon in soil: comparative results from monitoring in Lesvos Island and Ileia (Greece).* J Radioanal Nucl Chem. 299:203-219

**Perrier, F., Richon, P. & Sabroux, J.C.,** 2009. *Temporal variations of radon concentration in the saturated soil of Alpine grassland: The role of groundwater flow.* Sci Total Environ. 407:2361-2371

**Richon, P., Bernard, P., Labed, V., Sabroux, J.C., Beneïto, A., Lucius, D., Abbad, S. & Robe, M.C.,** 2007. *Results of monitoring 222Rn in soil gas of the Gulf of Corinth region*, Greece Radiat Meas. 42:87-93

**Steinitz, G. & Piatibratova, O.,** 2010a. *Radon signals in the Gavnunim intrusion, Makhtesh Ramon, Israel.* Geophys J Int. 180:651-665

**Steinitz, G. & Piatibratova, O.,** 2010b. *Radon signals at the Roded site, southern Israel.* Solid Earth. 1:99-109

**Steinitz, G., Kotlarsky, P. & Piatibratova, O.,** 2013. *Anomalous non-isotropic temporal variation of gamma-radiation from radon (progeny) within air in confined conditions.* Geophys J Int. 193:1110-1118

**Steinitz, G., Piatibratova, O. & Kotlarsky, P.,** 2011. *Possible effect of solar tides on radon signals.* J Environ Radioactiv. 102:749-765

**Sundal, A.V., Valen, V., Soldal, O. & Strand T.,** 2008. *The influence of meteorological parameters on soil radon levels in permeable glacial sediments.* Sci Total Environ. 389:418-28

**Szabó, K.Z., Jordan, G., Horváth, Á. & Szabó, C.,** 2013. *Dynamics of soil gas radon concentration in a highly permeable soil based on a long-term high temporal resolution observation series.* J Environ Radioactiv. 214:74-83

**Tukey, J.W.,** 1977. *Exploratory Data Analysis.* Addison-Wesley

**Velleman, P.F. & Hoaglin, D.C.,** 1981. *Applications, Basics and Computing of Exploratory Data Analysis.* Duxbury Press, Boston

**Weinlich, F.H., Faber, E., Bouskova, A., Horalek, J., Teschner, M. & Poggenburg, J.,** 2006. *Seismically induced variations in Marianske Lazne fault gas composition in the NW Bohemian swarm quake region, Czech Republic – a continuous gas monitoring.* Tectonophysics. 421:89-110

**WHO,** 2009. World Health Organization (WHO) *Handbook on Indoor Radon* – a Public Health Perspective: www.who.int/ionizing_radiation/env/radon/en/index1.html

**Winkler, R., Ruckerbauer, F. & Bunzl, K.,** 2001. *Radon concentration in soil gas: a comparison of the variability resulting from different methods, spatial heterogeneity and seasonal fluctuations.* Sci Total Environ. 272:273-282

**Woith, H., Barbosa, S., Gajewski, C., Steinitz, G.,**

**Piatibratova, O., Malik, U. & Zschau, J.,** 2011. *Periodic and transient radon variations at the Tiberias hot spring, Israel during 2000 – 2005.* Geochem J. 45:473-482

**Yan, R., With, H., Wang, R. & Wang, G.,** 2017. *Decadal radon cycles in a hot spring.* Sci Rep. 7:12120

Received at: 05. 03. 2020
Revised at: 21. 08. 2020
Accepted for publication at: 27. 08. 2020
Published online at: 28. 08. 2020